American Mineralogist, Volume 90, pages 1693–1704, 2005

Structure of framboidal pyrite: An electron backscatter diffraction study

HIROAKI OHFUJI,[1,*] ALAN P. BOYLE,[2] DAVID J. PRIOR,[2] AND DAVID RICKARD[1]

[1]School of Earth, Ocean, and Planetary Sciences, Cardiff University, Park Place, Cardiff CF10 3YE, U.K.
[2]Department of Earth Sciences, University of Liverpool, Liverpool L69 3GP, U.K.

ABSTRACT

The detailed crystallography of natural pyrite framboids has been determined for the first time using electron backscatter diffraction techniques. The crystallographic ordering of microcrystals correlates positively with morphological ordering; the crystallographic orientations are random in morphologically disordered framboids and are almost ordered in morphologically ordered framboids. Morphologically ordered framboids involve two types of systematic misorientations across the microcrystal boundaries: low-angle (ca. <20°) and high-angle (ca. 70–90°) misorientations. The low-angle misorientation probably reflects slight physical misalignment of microcrystals in the packing structure, whereas the high-angle misorientation is considered to result from the dichotomy of the pyrite microcrystals having fourfold morphological symmetry but only twofold crystallographic symmetry about <100>. Thus, the crystallographic orientation of microcrystals is not uniform, even in highly ordered framboids. This suggests that the self-organization of microcrystals in pyrite framboids is not crystallographically controlled, for example by sequential replication of existing microcrystals, since this would not result in high lattice misorientation angles between adjacent microcrystals. Presumably, the self-organization process is a consequence of the aggregation of multiple equidimensional and equimorphic microcrystals that have nucleated in a fixed volume. We suggest that the regular arrangement of microcrystals occurs by the physical rotation (reorientation) of individual microcrystals, driven by the reduction in surface free energy between neighbors.

INTRODUCTION

Pyrite framboids constitute one of the most remarkable forms of inorganic self-assembly found in nature. Ohfuji and Rickard (2005) defined the texture in terms of three specific attributes: (1) spheroidal to sub-spheroidal microscopic clusters (up to 250 μm) of (2) 10^3 to 10^6 discrete microcrystals of pyrite (FeS_2), and (3) which are basically all equant, equidimensional, and equimorphic (Fig. 1). Framboidal pyrite is ubiquitous in various geological environments, such as ancient sedimentary rocks of Archaean age (e.g., Hallbauer 1986), recent marine and lacustrine unconsolidated sediments (e.g., Sweeney and Kaplan 1973; Perry and Pedersen 1993), anoxic water columns (e.g., Ross and Degens 1974; Muramoto et al. 1991; Wilkin and Barnes 1997; Suits and Wilkin 1998), hydrothermal ore deposits (e.g., Kanehira and Bachinski 1967; Ostwald and England 1977; England and Ostwald 1993), and volcanic rocks (Love and Amstutz 1969). Similar framboid-like aggregates of microcrystalline pyrite have been produced experimentally (e.g., Sweeney and Kaplan 1973; Graham and Ohmoto 1994; Wilkin and Barnes 1996; Butler and Rickard 2000a; Ohfuji 2004; Ohfuji and Rickard 2005).

Pyrite framboids display two contrasting internal structures made up of constituent microcrystals: (1) an ordered structure (Figs. 1a and 1b) composed of the microcrystals that are arranged into an almost uniform morphological array and (2) a disordered structure (Fig. 1c) with no obvious internal ordering. In two-dimensional (2D) framboid sections, the microcrystal orderings are usually observed as cubic and hexagonal patterns (Love and Amstutz 1966; Kalliokoski and Cathles 1969; Rickard 1970; Ohfuji and Akai 2002) and as parallel linear patterns (Love and Amstutz 1966; Ohfuji 2004) in which the individual microcrystals have the same or very similar morphological orientations (Fig. 1a). The three-dimensional (3D) architecture of the regular microcrystal arrangements has been demonstrated from the morphological point of view as either (1) cubic close packing (ccp) or (2) icosahedral packing (Ohfuji and Akai 2002). Interestingly, these two packing structures are commonly observed in synthetic nano-scaled metal clusters of Au, Ag, and Pt particles (Spiegelmann and Poteau 1992; Lu and Tanaka 1997; Yacaman et al. 2001), which consist of densely packed atoms.

A major, and hitherto unanswered, question is what framboids (especially highly ordered framboids) actually are in crystallographic or materials science terms. There are no published studies on the crystallography of framboids. Butler (1994), in an unpublished Ph.D. study, reported the results of a single crystal X-ray diffraction (XRD) investigation of framboids. He reported sharp powder XRD patterns from individual pyrite framboids from the Rammelsberg deposit. The important result from Butler's work was that even framboids displaying well-defined internal microcrystal organization (ccp structure) were not simple single crystals in XRD terms. This was confirmed by a recent single-crystal XRD study of pyrite framboids (Ohfuji 2004). Both Butler (1994) and Ohfuji (2004) concluded that

*Present address: Geodynamics Research Center, Ehime University, Matsuyama 790-8577, Ehime, Japan. E-mail: ohfuji@sci.ehime-u.ac.jp

0003-004X/05/1112–1693$05.00/DOI: 10.2138/am.2005.1829

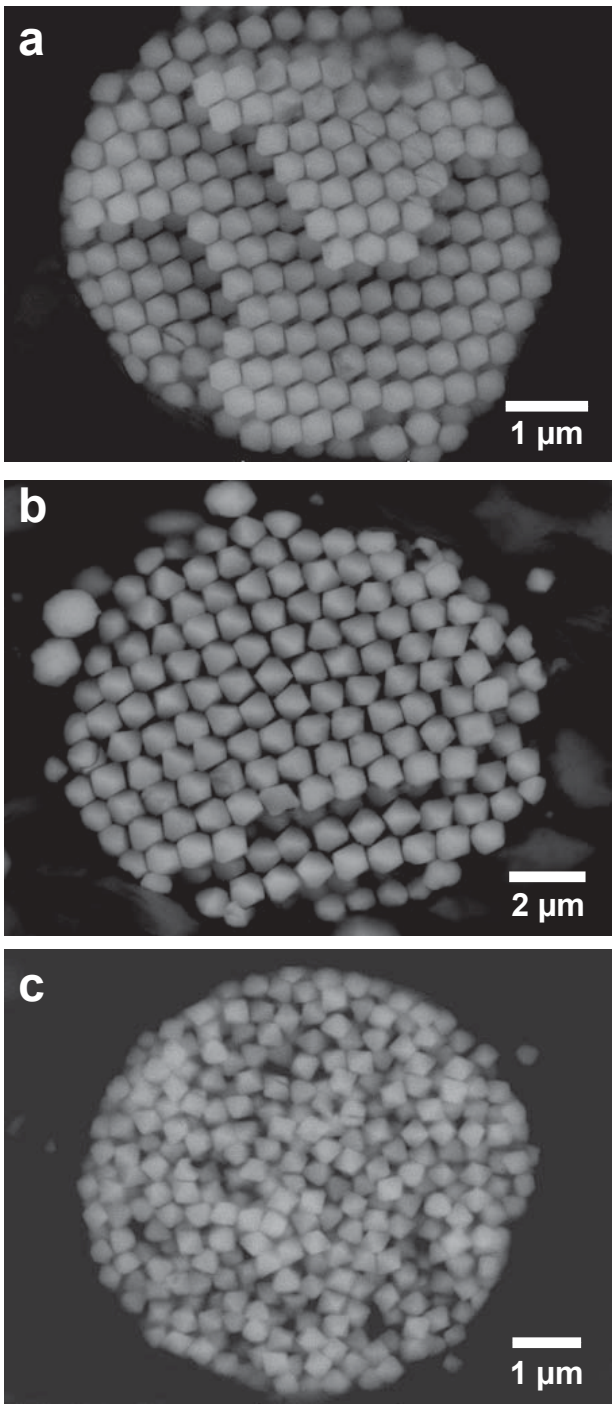

FIGURE 1. Backscattered electron images of typical regular and non-regular microcrystal organization observed in 2D sections of pyrite framboids from the Chattanooga shale. (**a**) Hexagonal arrangement made up of cubo-octahedral microcrystals, all of which share a common morphological orientation. (**b**) Hexagonal arrangements composed of octahedral microcrystals (with slight {100} truncation). Note that the morphological orientations of the microcrystals are not perfectly uniform; some are more or less misoriented from the orientation to which the majority belong. (**c**) Disordered structure composed of randomly aggregated octahedral microcrystals.

the framboid structure was composed of several single crystal domains composed of multiples of microcrystals all possessing the same crystallographic orientation. However, more detailed crystallographic information cannot be obtained by XRD.

This paper reports on an investigation aimed at determining the crystallographic nature of framboids. Recently, the SEM-based electron backscatter diffraction (EBSD) technique has been widely recognized as a powerful tool for investigating microstructures in geological materials (e.g., Prior et al. 1999). It allows acquisition of accurate crystallographic orientation information from an area that is not much larger than the electron probe size (i.e., a few tens of nanometers) on polished specimen surfaces (Prior et al. 1999, 2002; Spiess et al. 2001). The EBSD technique, coupled to orientation contrast (OC) imaging in the SEM, has been demonstrated to be useful for identifying evidence of plastic deformation in pyrite porphyroblasts (Boyle et al. 1998; Prior et al. 1999) and micro-scale textures and structures in polycrystalline pyrite, such as colloform and spongy aggregates (Freitag et al. 2004). In the present study these techniques were utilized for the first time to determine the crystallography of framboids. We used samples from the Devonian Chattanooga shale, which contains exceptionally highly ordered (ccp) framboids. The results have important implications for understanding how these inorganically self-organized natural materials form.

EXPERIMENTAL PROCEDURES

All framboids examined in this study are from the Chattanooga shale, which is a thin epicontinental (deep water) black shale sequence of late Devonian age, extending over vast areas of the North American craton (e.g., de Witt et al. 1993). The shale contains some of the best organized (ccp) pyrite framboids known (mostly <15 µm in diameter; Figs. 1a and 1b) (Love and Amstutz 1966; Butler 1994; Ohfuji 2004). The shale specimens were collected from 3889 km N, 655 km E, UTM zone 16S, Route 27, approximately 9 km north of Chattanooga, Tennessee, U.S.A. The specimens were cut into small blocks across the bedding planes; polished thin sections (100 µm in thickness) were made using conventional methods. The sections were polished a final time using SYTON fluid to remove the mechanical damage generated during the mechanical polishing process (Fynn and Powell 1979; Prior et al. 1996). A preliminary analysis of one of the polished sections with a very thin carbon coating encountered a serious charging problem due to the porous texture of the shale matrix, which consists mainly of anhedral quartz and fine clay minerals, such as illite. To solve this problem, the specimens were coated with gold-palladium, re-polished by SYTON to remove the coating on the polished surface layer (but leaving the cavities still coated with gold-palladium) and then were coated again with a very thin carbon layer. This process was found to reduce the charging problem significantly and also provided clear diffraction patterns.

EBSD analysis was performed using a CamScan X500 crystal probe SEM equipped with a thermionic field emission gun at the University of Liverpool. An accelerating voltage of 20 kV, a beam current of 20 nA, and a working distance of ca. 26 mm were used. The specimen lies horizontally in the SEM and the electron gun is inclined at 20°. EBSD patterns were collected from rectangular grid areas at a regular grid spacing of between 50 to 100 nm, depending on the size of the framboids and the constituent microcrystals. At each analyzed pixel, a diffraction pattern was acquired and Kikuchi bands were detected and indexed automatically using Channel 5.0 software from HKL Software. Crystallographic indexing was conducted only if more than eight detected Kikuchi bands corresponded with those contained in the standard reflector file for a pyrite crystal. Indexed points were saved to a file and plotted on an Euler-angle map which uses RGB (Red, Green, Blue) color intensity to represent the Euler-angle space (ϕ_1, Φ, ϕ_2, representing crystallographic orientations). Repetition of this analytical process provided a color orientation map from each selected grid area. Typically, about four points were analyzed per second. See Prior et al. (2002) for full details of the data collection methods.

The collected map data were processed using tools in the TANGO component of the CHANNEL 5.0 software as follows: (1) a noise-reduction filter was applied to remove single wild spikes; (2) extrapolation was used to rebuild grains for which only partial data were successfully collected; (3) systematic misindexing

was removed. The first and second processes were previously described in detail by Prior et al. (2002). The third process is needed to correct a misindexing error that can occur with pyrite. Although pyrite exhibits twofold symmetry in its [100] directions, it also exhibits fourfold pseudo-symmetry. This means that the EBSD patterns for two pyrite crystals at 90° to each other have the majority of Kikuchi bands in common (due to the fourfold pseudo-symmetry), and few that differ and define the true twofold symmetry. Two such patterns from adjacent pyrite microcrystals are shown in Figure 2. Most Kikuchi bands are the same, but some (arrowed) are different. The crystallographic significance of the differences is summarized by the Miller Index labels. During any experiment, an EBSD pattern is collected and image analysis software is used to choose the best eight bands in the pattern. If the eight bands do not include any of the bands diagnostic of the twofold <100> symmetry then there is the possibility of a systematic misindexing in which the solution is rotated 90° from the correct solution. Typically such misindexed data account for only a small minority (because the eight bands usually include at least one of the critical bands). They often occur as small domains at the edge or within a larger area with correct values, as will be discussed later. The TANGO software provides a way to for recognize and correct such errors.

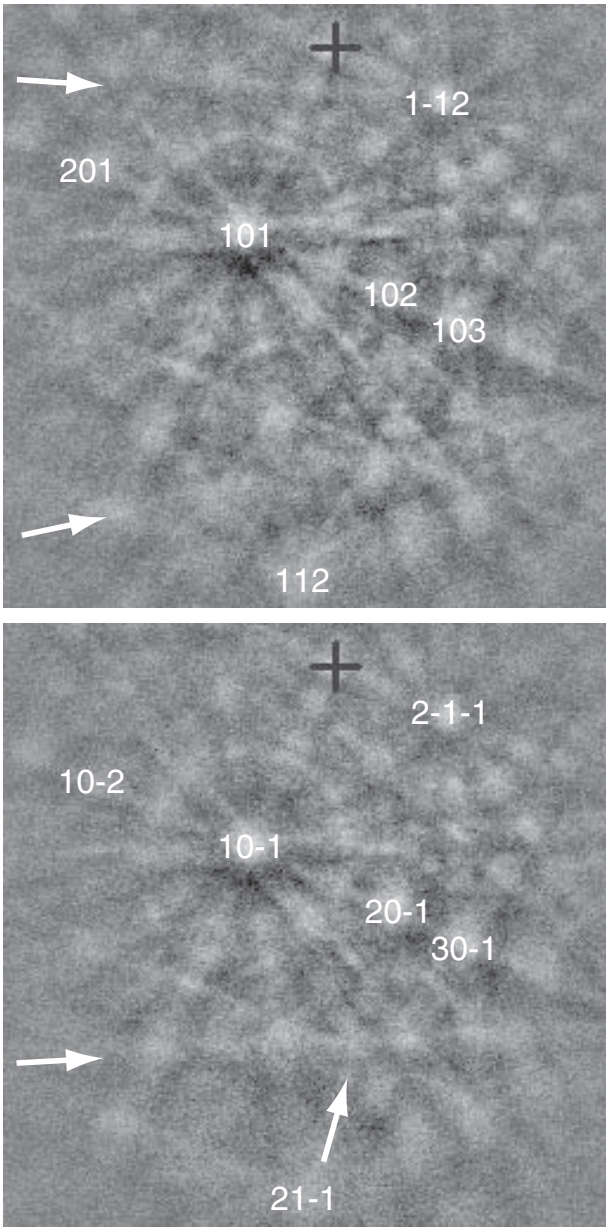

FIGURE 2. Two EBSD patterns with a 90° misorientation relationship (rotation around [010] axis). Note that although both patterns are very similar, the distributions of a few Kikuchi bands as indicated by arrows are clearly different in each pattern. If one of these bands is picked by the software and used for automatic indexing, the crystallographic orientation should be determined correctly. The patterns were collected manually from two adjacent microcrystals in an ordered pyrite framboid. The blue cross is the "pattern centre" used by the Channel 5.0 software.

RESULTS

Orientation contrast imaging

In well-polished framboid sections, the individual microcrystals were basically identified as discrete grains in both secondary electron (SE) and backscattered electron (BSE) images (Fig. 3a). They were recognized more clearly in orientation contrast (OC) images using forescatter detectors (Fig. 3b). Gray-scale OC is generated by the difference in BSE signal intensity, which varies with crystallographic orientation (Joy 1974; Lloyd 1987; Day 1993; Prior et al. 1996). Thus, the variation in the OC of the individual microcrystals (Fig. 3b) suggests that their crystallo-

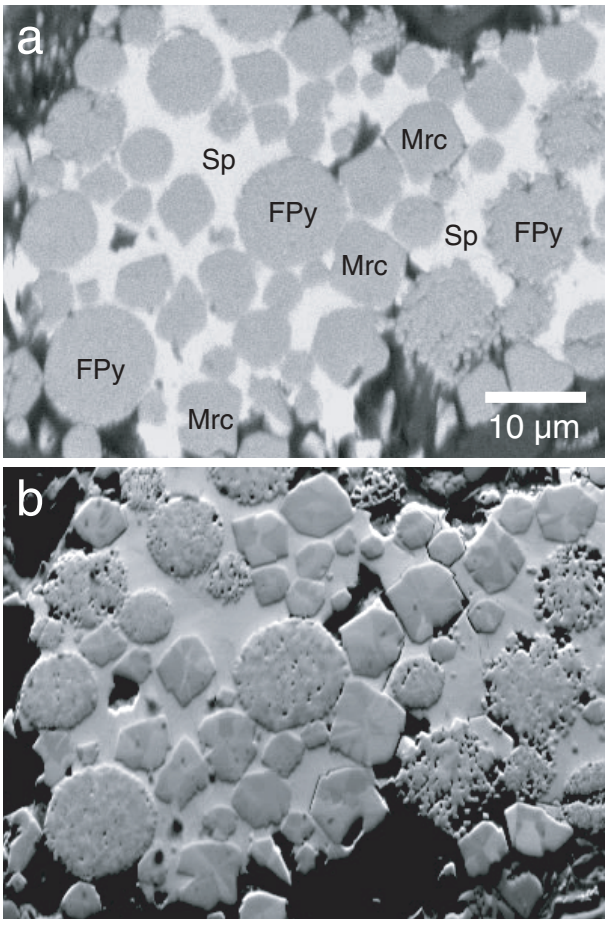

FIGURE 3. Backscatter *Z* contrast (**a**) and forescatter OC (**b**) images of pyrite framboids (FPy) occurring in a pyrite-marcasite (Mrc) clump enveloped by massive sphalerite (Sp). In the OC image, the grey-scale contrast shown by the framboidal microcrystals indicates that their crystallographic orientations are variable in each framboid. Euhedral marcasite crystals show a characteristic sectored structure.

graphic orientations are variable within one framboid. However, it should be noted that OC images are not quantitative (e.g., Day 1993; Prior et al. 1996; Trimby and Prior 1999). This means that high (or low) contrast does not simply reflect large (or small) difference in the crystallographic orientations.

Some pyrite framboids contained in the Chattanooga shale show solid internal structures in which the interstices between the microcrystals are entirely infilled with later pyrite (cf. Love and Amstutz 1966). Such framboid grains which have gone through later recrystallization were carefully excluded from the targets to be analyzed.

Orientation mapping

Pyrite framboids occurring in the Chattanooga shale were morphologically classified into two types: (1) ordered and (2) disordered framboids. In the former the microcrystals are regularly arranged in a cubic close packing (Figs. 1a and 1b), whereas in the latter they are randomly aggregated (Fig. 1c). In the Chattanooga shale used in this study approximately 30 to 40% of the framboids were observed to be morphologically ordered, which is consistent with the previous reports by Love and Amstutz (1966) and Amstutz et al. (1967). More than twenty sets of complete orientation maps were collected from both types of framboids. Typical examples of map data sets collected from disordered and highly ordered framboids are shown in Figure 4. Figure 4a shows a band contrast image obtained from a disordered framboid. The band contrast image represents a quantitative image analysis parameter of the EBSD pattern quality (cf. Prior et al. 2002). Basically, dark pixels have poor pattern quality, whereas bright pixels have good pattern quality. The image shows that the boundaries between individual microcrystals have relatively poor pattern quality due to the discontinuous physical gaps involved. Figure 4b shows an unprocessed original color orientation map obtained from the framboid. Note that individual microcrystals are indicated by an almost uniform color intensity, suggesting that they are single crystal grains, although the map leaves non-indexed pixels (shown as white pixels) along microcrystal boundaries and small domains of 90°-misindexed pixels (shown with a different color intensity) in some microcrystals (Fig. 4b). To investigate the misorientation magnitude involved between adjacent microcrystals, the raw map data were processed by the methods described above without introducing artifacts so that most of the microcrystals are in contact with each other (Fig. 4c). In the processed map (Fig. 4c), the range of colors shown by different individual microcrystals (Fig. 4c) suggests that their crystallographic orientations are not uniform. This is clearly recognized in the pole figures, on which pyrite orientations <100>, <110>, and <111> from the whole analyzed data set are plotted (Fig. 4d), showing no obvious crystallographic preferred orientation (CPO). In other words, the microcrystals that constitute morphologically disordered framboids appear to have crystallographically random orientations.

Figures 4e, 4f, and 4g show a band contrast image and unprocessed/processed orientation maps collected from a highly ordered framboid, in which the microcrystals are arranged in a hexagonal pattern (Fig. 4e). The orientation maps (Figs. 4f and 4g) display less color variation than those collected from disordered framboids (Fig. 4c): most of the microcrystals are colored orange or pink, suggesting that the crystallographic orientations of the microcrystals are less variable. The pole figures obtained from the morphologically ordered framboid indicate that there are two very strong CPOs with respect to the microcrystal arrangements (Fig. 4h). They are not distinguishable in the <100> and <110> pole figures, but are clearly visible as separate concentrations of different-colored plots (pink and orange) in the <111> pole figure (Fig. 4h). This phenomenon is interpreted as a function of high-angle (~90°) misorientations observed in ordered framboids, as is discussed below. The pole figures also show that some of the dark blue and dark brown microcrystals deviate from the main CPOs (Fig. 4h). Although such microcrystals are mostly distributed randomly on the framboid section, some of them are adjacent to each other (Fig. 4g).

All the pyrite framboids analyzed in this study were found to have either no CPOs or strong CPOs (Fig. 5). These different crystallographic features are apparently associated with the internal microcrystal structures; the former were obtained from morphologically disordered framboids (Fig. 4a), whereas the latter were obtained from morphologically ordered framboids (Fig. 4e). Although both types of framboids (with or without strong CPOs) were observed in small local areas, at smaller scales their occurrences might be distinguishable, as indicated in Figure 5, where five framboids with strong CPOs are located close to each other, but at distances from the framboids with random CPO. This may imply that the two types form under slightly different local conditions or time periods.

For morphologically ordered framboids, there is a systematic relationship between the 2D views (patterns) of the microcrystal arrangements displayed in framboid sections and their CPOs. In sections where the microcrystals are arranged in a cubic array, one of the CPO axes obtained is plotted around the centre of the <100> pole figure (Fig. 5a). In sections where the microcrystals are arranged in a hexagonal array, one of the CPO axes is plotted around the centre of the <110> or <111> pole figure (Fig. 4h). This means that in the cubic array, the individual microcrystals orient their <100> directions perpendicular to the plane of the microcrystal array, whereas in the hexagonal array, the microcrystals are oriented with <110> or <111> vertical. This result is in good agreement with the observation of Ohfuji (2004), who demonstrated the microcrystal orientation in the ccp structure based on microcrystal habit.

Microcrystal misorientation in framboids

Quantitative analysis of misorientation between two grains of the same mineral associated with various geological textures, such as in tectonites, metamorphic rocks, and igneous rocks, is important to investigate the microstructural features and their formation processes (Wheeler et al. 2001). The degree of misorientation is basically expressed by a rotation axis and rotation angle. Figure 6 shows misorientation angle distributions (> 2°) calculated between neighboring pairs (of pixels analyzed) and from random pairs in the disordered (Fig. 4c) and ordered (Fig. 4g) framboids after data processing. In the disordered framboids, the misorientation angle distributions of both neighboring pairs and random pairs roughly correspond to a theoretical random orientation distribution indicated by a dotted line, although low-angle (5 to 25°) and high-angle (75 to 90°) misorientations from

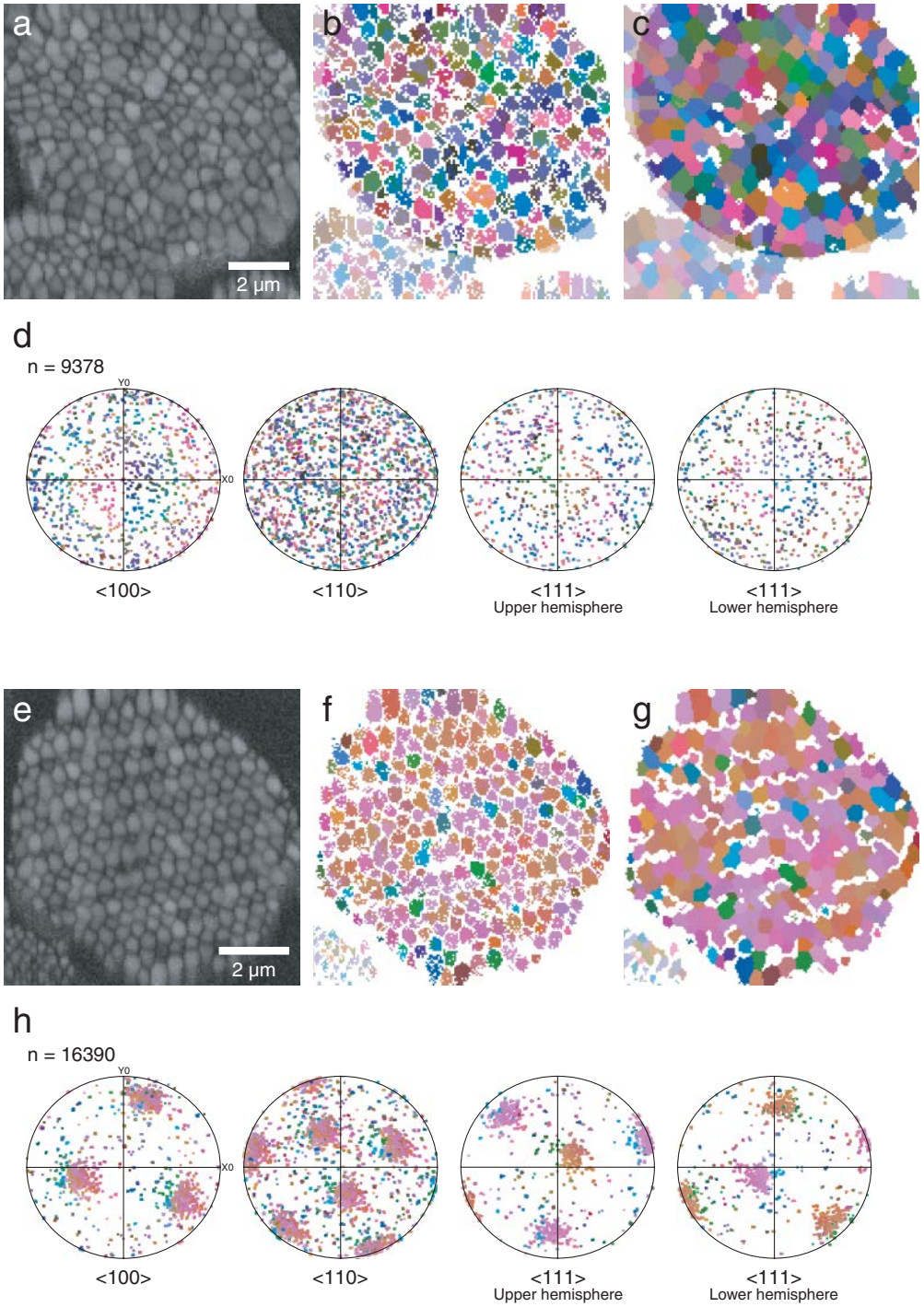

FIGURE 4. Band contrast images, orientation maps, and corresponding pole figures for morphologically disordered (**a**-**d**) and ordered (**e**-**h**) pyrite framboids. Band contrast images (**a**, **e**) are constructed from all EBSD patterns collected from the analyzed areas. Dark pixels have poor pattern quality, whereas bright pixels have good pattern quality. Original orientation maps (**b**, **f**) have non-indexed white pixels along the boundaries of individual microcrystals and small domains of misindexed pixels (seen as different color intensity) in some microcrystals. In the processed maps (**c**, **g**), such non-indexed pixels have been occluded by digital extrapolation and misindexed pixels have been corrected by the process described in the text. As a consequence, most of the microcrystals are in contact with each other, which allows investigation of the misorientation magnitude involved between microcrystal boundaries. The crystallographic orientations of all the analyzed pixels are plotted in upper hemisphere pole figures (**d**, **h**). The crystallographic orientation data collected from a single crystal give three directions defined by [100], [010], and [001] in the <100> pole figure, six directions defined by [110], [101] [011], [1$\bar{1}$0], [$\bar{1}$10], and [$\bar{1}\bar{1}$0] in the <110> pole figure, and four directions defined by [111], [1$\bar{1}$1], [$\bar{1}$11], and [$\bar{1}\bar{1}$1] in total in both (upper and lower hemisphere) <111> pole figures.

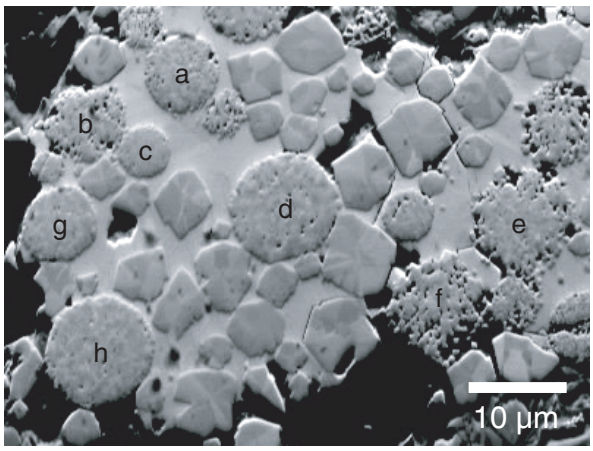

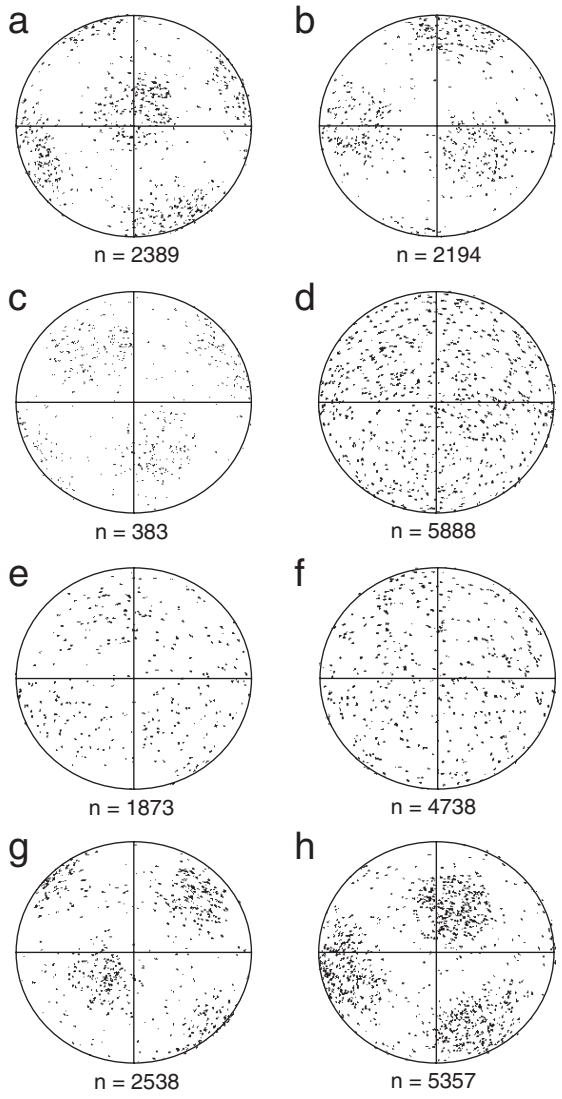

FIGURE 5. Upper hemisphere <100> pole figures obtained from eight pyrite framboids contained in a pyrite-marcasite clump (Fig. 3). The pole figures indicate strong CPO (**a**, **b**, **c**, **g**, **h**), weak CPO (**e**), and random CPO (**d**, **f**). Note that the five framboids with strong CPO are located near the edge of the pyrite-marcasite clump.

neighboring pairs occur somewhat more frequently (Fig. 6a). On the other hand, the misorientation angle distribution obtained from the ordered framboid has two peaks at 10-15° and 80-85° for neighboring pairs and at 10-15° and 75-80° for random pairs, and middle-angle misorientations (between 25 and 60°) are far less frequent (Fig. 6b). Such twin peaks in the misorientation angle distribution were commonly observed in all the morphologically ordered framboids analyzed with strong CPOs, although some of them show somewhat broader peaks (Figs. 5b and 5c; low-angle: 2 to 35°, high-angle: 55 to 90°). The abundance of such low-angle and high-angle misorientations can also be seen in the pole figures (Fig. 4h). The low-angle misorientations are indicated by the small scattering of the CPO axes plotted, and

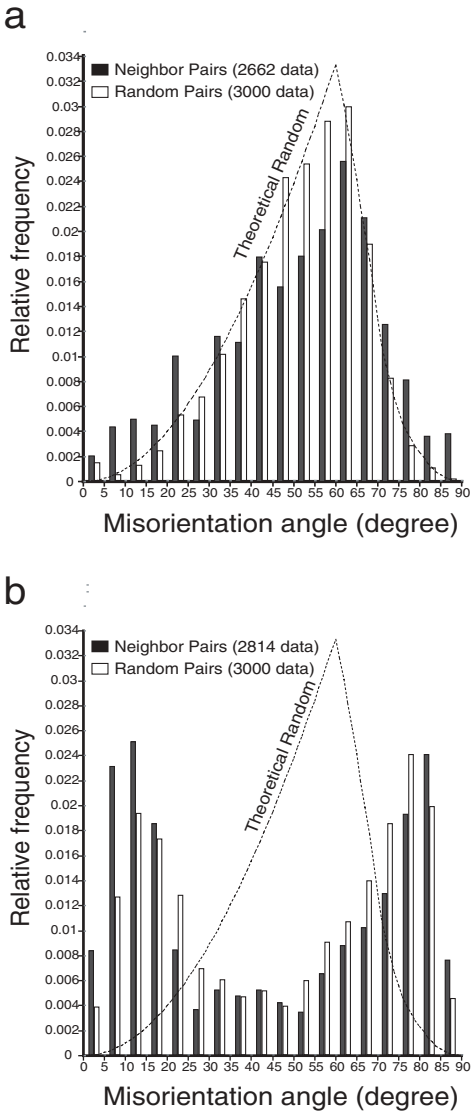

FIGURE 6. Misorientation angle distributions (>2°) calculated between neighboring pairs (of analyzed pixels) and between random pairs from the (**a**) disordered and (**b**) ordered framboids, after data processing (calculated from the processed map, Figs. 4c and g, respectively). The dotted line indicates the expected distribution for a random orientation distribution (Grimmer 1980).

the high-angle ones are recognized in the <111> pole figure as a separate CPO indicated by different colored plots as described above (Fig. 4h). The reason why the high-angle misorientations are not clearly visible in the <100> and <110> pole figures is related to the cubic symmetry of pyrite. Since, in cubic crystals, the angle between <100> zone axes and between <110> are both 90°, the distributions of the <100> and <110> orientations are almost identical before and after high-angle (~ 90°) rotation, whereas distribution of <111> does change.

Figure 7 shows misorientation profiles across parts of arranged microcrystals in the ordered framboids (Figs. 4e and 7a). Note that the orientations of the analyzed pixels do not change within individual microcrystals (strictly speaking, variations <2°) as indicated by the flat-topped peaks and flat troughs (Figs. 7b, 7c, and 7d left), but they change abruptly across the boundaries between microcrystals (Figs. 7b–d). The misorientation (rotation) axes from neighboring pairs obtained from the ordered framboid (Fig. 4g) were plotted as inverse pole figures with different misorientation angles divided into 10° ranges (Fig. 8). Figure 8 indicates that low-angle misorientation axes (2 to 20°) are distributed more or less randomly, while higher angle misorientation axes (60 to 90°) tend to concentrate around [001] with increasing misorientation angle. The middle-angle misorientation axes (20 to 60°) are scattered as a whole, but also show concentrations of many dots within narrow areas (Fig. 8). There are relatively few microcrystals with intermediate misorientation angles (i.e., 20 to 60°); they tend to be dark blue and dark brown in the processed orientation map (Fig. 4g). These have very variable misorientation axes (Fig. 8). The local clustering of axes for these is a function of the software calculating misorientation axes for several pairs of adjacent pixels on the same grain boundary, and thus, reflecting the slight variation (typically, < 1 ~ 2°) in crystallographic orientation.

For the reason mentioned above, high-angle (90°) misorientations could possibly be produced by computational misindexing of diffraction patterns with the CHANNEL 5.0 software. However, the almost uniform color intensity displayed within each microcrystal in the unprocessed orientation maps (Figs. 4b and 4f) suggests that the occurrence of such systematic misindexing errors is very minor. Furthermore, we manually examined EBSD patterns collected from adjacent pairs of microcrystals that give a 90° misorientation relationship and confirmed that the large misorientations are truly intrinsic to the microcrystal structures (Figs. 2a and 2b).

Discussion

Crystallographic nature of framboids

EBSD analysis indicates that crystallographic ordering of microcrystals correlates positively with morphological ordering as indicated by CPOs plotted in the pole figures (Figs. 4d and 4h). However, even in morphologically highly ordered framboids (Fig. 4e), the microcrystals commonly involve two types of crystallographic misorientations between microcrystals: low-angle (2 to 20° in average) and high-angle (70 to 90° in average) misorientations (Figs. 6–8).

Low-angle crystallographic misorientations have been reported as being common in pyrite crystals that have deformed by dislocation glides (e.g., Boyle et al. 1998; Prior et al. 1999) and are also involved in the radiating growth of acicular pyrite crystals (e.g., Freitag et al. 2004). Both the deformation and the growth cases can be described by a lattice rotation around a specific axis, demonstrated in pole figures and misorientation axis distribution diagrams (cf. Freitag et al. 2004). However, the rotation axes for the low-angle misorientations observed in ordered framboids indicate completely random distribution (Fig. 8), suggesting that the misorientations are not systematic. Thus, it seems unlikely that the misorientations are derived from deformation of whole framboids or some peculiar growth feature of the individual microcrystals. A detailed morphological study of framboidal microcrystals by Ohfuji (2004) showed that even highly ordered pyrite framboids commonly have slight misalignments in the microcrystal coordination (Figs. 1a and 1b). The occurrence of the low-angle misorientations in morphologically ordered framboids probably reflects such physical misalignment of the microcrystals.

On the other hand, the rotation axes for the high-angle microcrystal misorientations observed in morphologically ordered framboids are systematic and almost parallel to the <100> zone axes (Fig. 8), i.e., the crystal axes of pyrite. Pyrite twins on {110} faces with a [001] twin axis, but only by interpenetration. If such a twinning relationship existed among individual framboidal microcrystals, it would not provide the observed high-angle misorientations. It is worthy of note that, despite the abundance of such misorientations, the morphological orientations of the individual microcrystals are indeed almost uniform (Figs. 1a and 1b). This suggests that high-angle misorientations in ordered framboids are closely related to the geometric and symmetrical features of the constituent microcrystals.

The microcrystals in ordered framboids from the Chattanooga shale are almost exclusively truncated-octahedra and octahedra (Fig. 1; cf. Ohfuji 2004), both of which morphologically possess fourfold axes in the <100> zone axes (Fig. 9). This means that 90° rotations around any <100> direction provide morphologically identical orientations. However, in crystallography, the symmetry involved in the <100> directions in pyrite is not fourfold, but twofold. This low symmetry of the pyrite structure (space group *Pa*3) is attributed to the dumbbell-like arrangement of S atoms in the NaCl-type structure (Fig. 10). The twofold symmetry means that the [100], [010], and [001] zone axes (i.e., crystallographic axes, *a, b, c*) of pyrite are crystallographically not interchangeable with each other by a simple 90° rotation as in simple cubes. Accordingly, a 90° rotation of a pyrite microcrystal around the <100> axes directly generates 90° crystallographic misorientations, although their morphological orientation in the packing stays effectively the same. Thus, the data suggest that for ordered framboids, the morphological misalignment is typically 0-20°, whereas the crystallographic misalignment is 0–20° or 70–90° reflecting the presence of both low- and high-angle misorientations due to the <100> axes being diads, not tetrads.

The 90° misorientation involving many microcrystals in ordered framboids cannot be generated by crystallographic operations (even by twin relationships), as mentioned above. Therefore, the self-organization of microcrystals in pyrite framboids is not a consequence of a crystallographically controlled process such as extreme skeletal or dendritic crystal growth (cf. Butler 1994; Butler and Rickard 2000b).

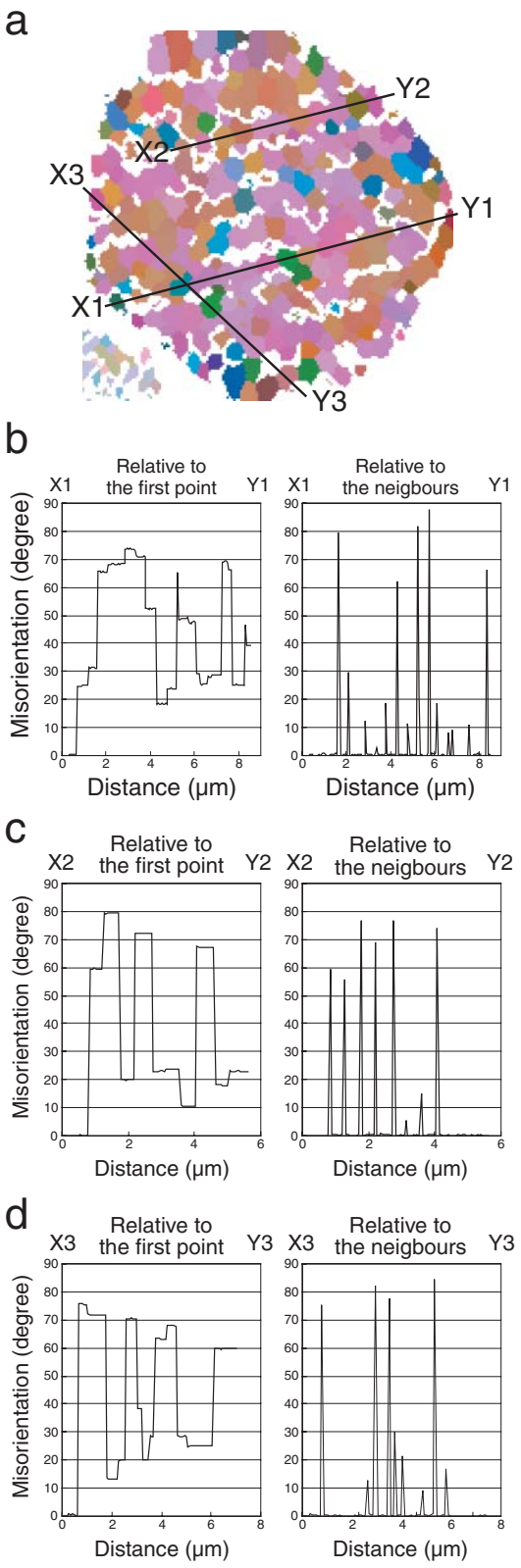

FIGURE 7. Misorientation profiles across (**b**) X1-Y1, (**c**) X2-Y2, and (**d**) X3-Y3 sections through the processed orientation map [(**a**); the same as Fig. 4g] obtained from the ordered framboid.

Implication for the self-organization process

Amstutz et al. (1967) investigated the orientation of morphologically ordered pyrite framboids in the Chattanooga shale using a conventional stereographic method. They reported a preferred orientation of ordered framboids in the shale and claimed that self-organization of framboidal microcrystals might originate from crystal growth during compaction of the surrounding sediments. However, the orientation measurements conducted by Amstutz et al. (1967) do not reflect a substantial degree of framboid orientation. The orientation data were collected from only 10–20% of total pyrite framboids in the shale, which showed clear linear arrangement of microcrystals in polished sections (see Figs. 1a, b in Amstutz et al. 1967), while another 30–40% of framboids in the sections also displayed obvious internal microcrystal ordering, although they lacked any distinct lineation (Amstutz et al. 1967). Therefore, Amstutz et al.'s (1967) conclusion that ordered framboids have a common preferred orientation in the shale was erroneous. Our EBSD-based crystallographic orientation data collected from the microcrystals that constitute ordered framboids confirm that there is no obvious preferred orientation of ordered framboids in the shale (Fig. 5). In addition, regular arrangements of microcrystals are also observed in pyrite framboids from recent unconsolidated sediments (e.g., Stakes et al. 1999; Böttcher and Lepland 2000; Large et al. 2001). Therefore, it seems unlikely that the self-organization of framboidal microcrystals occurs in response to compaction of the surrounding sediments.

This EBSD study also indicates that microcrystal self-organization in pyrite framboids is not a function of crystallographically controlled growth, since such a mechanism would not result in near-90° misorientations between adjacent microcrystals. An alternative mechanism involves the aggregation of many equidimensional microcrystals nucleated in a fixed volume. Given a framework composed of regularly arranged microcrystals it might be supposed that a new microcrystal would accommodate coherently in each site (void space) in an attempt to achieve morphological conformity. However, the observed regular arrangement of octahedral microcrystals is relatively loose, containing large gaps or pore spaces between microcrystals (Fig. 1b). Thus, the combination of regular organization and high-angle misorientation of microcrystals in ordered framboids indicates that the organizing mechanism cannot just be either morphological packing or crystallographic ordering.

We consider that the self-organization process reflects the overall development of an energetically more stable state in framboidal aggregates. Framboidal microcrystals are colloidal-sized and therefore have a high surface area relative to their volume. This, in turn, means that the total surface free energy associated with individual microcrystals can be lowered by particle aggregation or recrystallization (grain growth) (cf. Wilkin and Barnes 1997). The two fundamental factors in the self-organization process are: (1) reduction of the surface free energy associated among individual microcrystals and (2) minimization of the total surface free energy associated with whole framboidal aggregates. These factors are satisfied by introducing the densest packing structures, cubic close packing and icosahedral packing structures. The nature of these packings has been studied using 13-sphere packing models, in which a sphere is surrounded by the

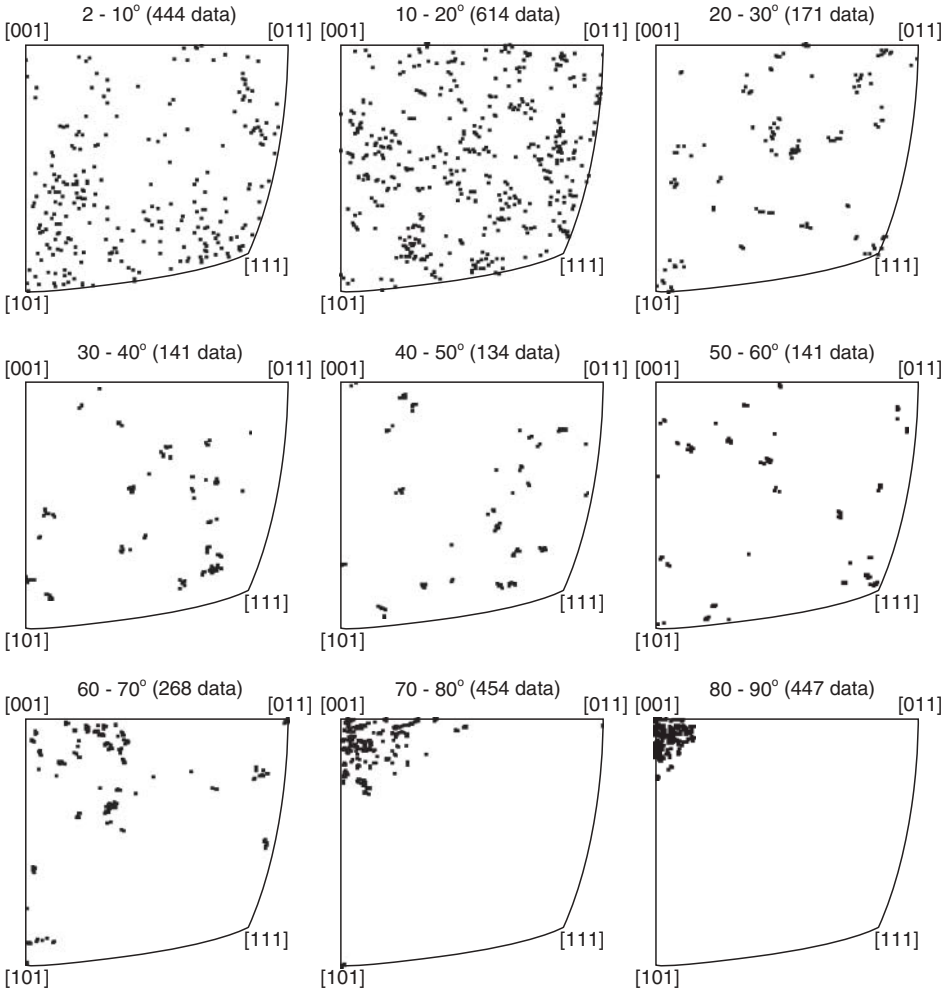

FIGURE 8. Misorientation axes distribution plotted in inverse pole figures at misorientation angle ranges of 10°. See text for details.

maximum number (twelve) of nearest neighbors (Ohfuji 2004). Such two-sphere coordinations (cubic close and icosahedral packings) are expected to minimize the repulsions between each sphere while maintaining high symmetry. If framboidal microcrystals were all identical spheres, the ordering may be explained by such packing. However, in practice, microcrystals are pyrite single-crystals which have morphological and crystallographic orientations as mentioned above. Thus, the surface energy involved is expected to not be equant, and is influenced by both morphological and crystallographic configurations. We suggest that with respect to the reduction in the surface energy associated with microcrystals, the reorientation of microcrystals (i.e., the ordering process) may play an important role during framboid formation.

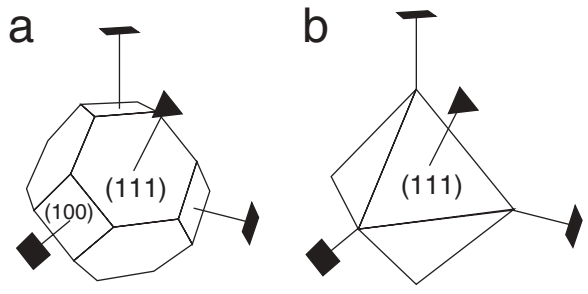

FIGURE 9. Morphological symmetry involved in (**a**) a truncated octahedron and (**b**) a simple octahedron. Both have fourfold axes along <100> directions and threefold axes along <111> directions.

Spiess et al. (2001) and Prior et al. (2002) studied garnet porphyroblasts occurring in Paleozoic mica schists using the EBSD technique and found that some aggregates of garnet grains have very strong CPO. They proposed a model involving: (1) simultaneous nucleation of randomly oriented seed crystals in a fixed volume; (2) growth and weak clustering of garnet grains with physical rotations of individual grains (induced by impingement), which provides a weak CPO for each cluster; (3) further growth and coalescence of individual grains with continuing grain rotations, which considerably increases the degree of the bulk CPO; and (4) final growth (Spiess et al. 2001; Prior et al. 2002). They suggested that the physical relative rotations of individual grains occur to reduce misorientation magnitude at the boundaries between adjacent garnets and that the process is driven by reduction in total surface energy (boundary energy),

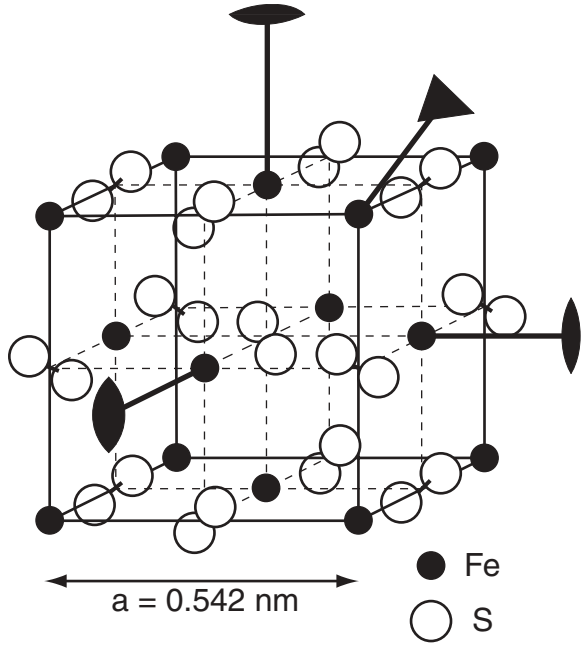

FIGURE 10. The crystal structure of pyrite (modified after Strunz 1957). Pyrite has an NaCl-like cubic structure in which Fe atoms are located at the corners and face centers of the cube and S atoms arranged in "dumb-bell" pairs are at the cube centre and the midpoints of cube edges (Fig. 9). The structure has threefold axes along <111> directions and twofold axes along <100> directions.

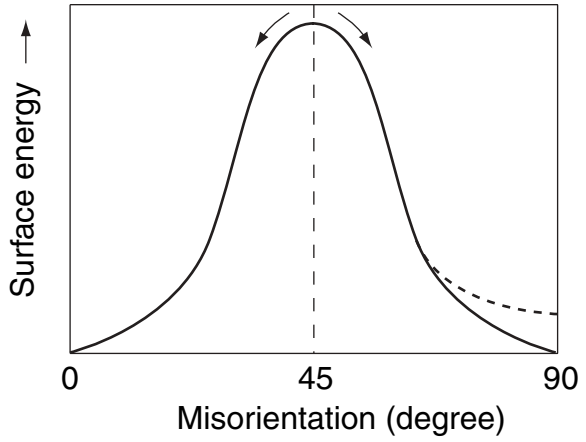

FIGURE 11. Schematic figure showing expected surface energy configuration as a function of misorientation for boundaries between pyrite microcrystals in framboids. The surface energy increases from 0 at 0° misorientation to a maximum at middle-angle misorientation and decreases toward 90° misorientation. The bilateral symmetry of the misorientation angle distribution histogram for morphologically ordered framboids (Fig. 6b) suggests the surface energy maximum is probably around 45° misorientation. Although 90° misorientation is energetically favored as observed, the corresponding surface energy state may not be the same as that with 0° misorientation, but may be somewhat higher as indicated by the dotted line.

which is a complex function of boundary misorientation, and is generally lower for smaller misorientations (Sutton and Baluffi 1987; Spiess et al. 2001). Some experimental studies based on rotating ball experiments (Herrmann et al. 1976; Sauter et al. 1977; Erb and Gleiter 1979) demonstrated that the reduction in surface energy can act as a driving force to reduce crystallographic misorientations (see also Spiess et al. 2001). A similar situation may occur in the microcrystal self-organization process in pyrite framboids. During the aggregation of a proto-framboid, initially randomly oriented microcrystals reorient themselves on impingement so that the associated surface energy is minimized. Generally, pyrite framboids precipitate from aqueous fluids such as occur in sediment pore spaces and the water column (e.g., Raiswell and Berner 1985; Muramoto et al. 1991; Suits and Wilkin 1998). This setting should allow microcrystals to rotate relatively freely, ideally toward a configuration with minimum crystallographic misorientation angle (i.e., 0°), but practically producing slight microcrystal misalignment (i.e., low-angle misorientations). However, we have shown that microcrystal rotations are equally likely toward 90° misorientation. This implies that the 90° misorientation configuration has the same or similar relatively low surface energy minimum as the 0° misorientation configuration does (Fig. 11). Studies based on experimental measurements of boundary energy in metals (Chan and Baluffi 1985; Sutton and Baluffi 1987), semiconductors (Babcock and Vargas 1995), and ceramics (Saylor and Rohrer 1999) have shown the presence of energy minima associated with specific boundary orientations such as twins or coincident site-lattice orientations (cf. Humphreys and Hatherly 1995), although boundary energy generally increases from zero at zero misorientation. The abundance of the high-angle misorientations in ordered framboids suggests that the high and low-angle misorientation relationships of the microcrystals are probably equally energetically favored.

From the foregoing, we propose that the self-organization of pyrite microcrystals in framboids occurs by (1) nucleation of microcrystals all with similar size and shapes in a fixed volume; (2) aggregation of the randomly oriented microcrystals driven by surface forces and the reduction in total surface energy associated with both the individual microcrystals and the whole aggregate, resulting in the formation of a spheroidal shape to the body as a whole; and (3) reorientation of the microcrystals driven by further reduction in surface energy associated with the grain boundaries, resulting in the formation of regular organization. This three-step formation mechanism of organized pyrite framboids is similar to the process originally proposed by Wilkin and Barnes (1997), which was based on (1) the simultaneous nucleation of several colloidal-sized ferrimagnetic greigite, Fe_3S_4, microcrystals; (2) subsequent growth and aggregation of the particles to form a spheroidal volume of organized microcrystals under the influence of various interaction forces including magnetic, electrostatic, and van der Waals forces; and (3) subsequent transformation of the greigite to pyrite. In contrast, ferrimagnetic particles are not a prerequisite for self-organization in the process determined in the present study, which is consistent with previous reports on the experimental synthesis of pyrite framboids in the absence of greigite (e.g., Butler and Rickard 2000a). We suggest that disordered framboids (Fig. 1c) result from aggregates that have not attained a minimum energy configuration. Whether framboids can achieve the regular microcrystal arrangement during the formation process may be related to a function of relative

nucleation and crystal growth rates of individual microcrystals and other physicochemical conditions in the local formation site. For example, relatively fast growth rates may cause microcrystals to impinge on each other before significant rotation can take place.

Self-organization driven by reduction in surface energy may also be favored by microcrystalline particles that are all equidimensional and equimorphic (i.e., having similar surface properties) and were precipitated in a certain volume. This could explain the development of regular ordering observed in irregular masses of non-framboid-forming microcrystalline pyrite grains from many sedimentary deposits (Sawlowicz 2000; Jiang et al. 2001; McKay and Longstaffe 2003), regular alignments of several microcrystalline pyrite grains (Kawamura, in prep.), and partial microcrystal ordering in some framboids (e.g., Rickard 1970; Butler 1994; Ohfuji and Rickard 2005). If all the conditions required are not satisfied, the microcrystal ordering is not perfect, leaving relatively large ranges of misorientations observed even in regularly packed (ccp) framboids (Fig. 1b).

Such aggregation-driven self-organization appears to provide a novel mechanism for the synthesis of regular 3D micro-arrays of semi-conductor materials.

ACKNOWLEDGMENTS

We thank J. Mies of the University of Tennessee, Chattanooga, for providing the specimens used in this study. We also acknowledge N. Shimobayashi and Y. Seto of Kyoto University for their help and suggestions about preliminary EBSD analysis and L. Badham of Cardiff University for his useful advice in preparing the polished sections used in this study. This work was funded by NERC grant NER/L/S/2000/00611 to D.R. and an ORS award to H.O. Analytical work in Liverpool was supported by NERC grant NERC/A/S/2001/01181 to D.P. and A.B.

REFERENCES CITED

Amstutz, G.C., Park, W.C., and Schot, E.H. (1967) Orientation of framboidal pyrite in shale. Mineralium Deposita, 1, 317–321.

Babcock, S.E. and Vargas, J.L. (1995) The nature of grain boundaries in the high T_c superconductors. Annual Review of Material Science, 25, 193–222.

Böttcher, M.E. and Lepland, A. (2000) Biogeochemistry of sulphur in a sediment core from the west-central Baltic Sea: Evidence from stable isotopes and pyrite textures. Journal of Marine Systems, 25, 299–312.

Boyle, A.P., Prior, D.J., Banham, M.H., and Timms, N.E. (1998) Plastic deformation of metamorphic pyrite: new evidence from electron-backscatter diffraction and forescatter orientation-contrast imaging. Mineralium Deposita, 34, 71–81.

Butler, I.B. (1994) Framboid formation. Ph.D. Thesis. Cardiff University, U.K.

Butler, I.B. and Rickard, D. (2000a) Framboidal pyrite formation via the oxidation of iron (II) monosulfide by hydrogen sulphide. Geochimica et Cosmochimica Acta, 64, 2665–2672.

——— (2000b) Framboidal pyrite: Self-organisation in the Fe-S system. Journal of Conference Abstracts, 5, 276–277.

Chan, S. and Baluffi, R.W. (1985) Study of energy vs misorientation for grain boundaries in gold by crystallite rotation method—I. [001] twist boundaries. Acta Metallurgica, 6, 1113–1119.

Day, A. (1993) Developments in the EBSP technique and their application to grain imaging. Ph.D. Thesis, University of Bristol.

de Witt, W., Roen, J.B., and Wallace, L.G. (1993) Stratigraphy of Devonian black shales and associated rocks in the Appalachian Basin. U.S. Geological Survey Bulletin, 1909-B, 1–57.

England, B.M. and Ostwald, J. (1993) Framboid-derived structures in some Tasman fold belt basemetal sulphide deposits, New South Wales, Australia. Ore Geology Reviews, 7, 381–412.

Erb, U. and Gleiter, H. (1979) The effect of temperature on the energy and structure of grain boundaries. Scripta Metallurgica, 13, 61–64.

Freitag, K., Boyle, A.P., Nelson, E., Hitzman, M., Churchill, J., and Lopez-Pedrosa, M. (2004) The use of electron backscatter diffraction and orientation contrast imaging as tools for sulphide textural studies: example from the Greens Creek deposit (Alaska). Mineralium Deposita, 39, 103–113.

Fynn, G.W. and Powell, W.J.A. (1979) The cutting and polishing of electro-optic materials. Adams Hilger, London.

Graham, U.M. and Ohmoto, H. (1994) Experimental study of formation mechanisms of hydrothermal pyrite. Geochimica et Cosmochimica Acta, 58, 2187–2202.

Grimmer, H. (1980) A unique description of the relative orientation of neighbouring grains. Acta Crystallographica, A36, 382–389.

Hallbauer, D.K. (1986) The mineralogy and geochemistry of Witwatersrand pyrite, gold, uranium and carbonaceous matter. In C.R. Anhaeusser and S. Maske, Eds., Mineral Deposits of Southern Africa, p. 731–752. Geological Society of South Africa.

Herrmann, G., Gleiter, H., and Baro, G. (1976) Investigation of low energy grain boundaries in metals by a sintering technique. Acta Metallurgica, 24, 353–359.

Humphreys, F.J. and Hatherly, M. (1995) Recrystallization and related annealing phenomena. Pergamon Press, Oxford.

Jiang, W.-T., Horng, C.-S., Roberts, A.P., and Peacor, D.R. (2001) Contradictory magnetic polarities in sediments and variable timing of neoformation of authigenic greigite. Earth and Planetary Science Letters, 193, 1–12.

Joy, D.C. (1974) Electron channeling patterns in the SEM. In D.B. Holt, M.D. Muir, I.M. Boswarva, and P.R. Grant, Eds., Quantitative Scanning Electron Microscopy. Academic Press, New York.

Kalliokoski, J. and Cathles, L. (1969) Morphology, mode of formation, and diagenetic changes in framboids. Bulletin of the Geological Society of Finland, 41, 133–153.

Kanehira, K. and Bachinski, D. (1967) Framboidal pyrite and concentric textures in the ores of the Tilt Cove mine, Northeastern Newfoundland. Canadian Mineralogist, 9, 124–128.

Large, D.J., Fortey, N.J., Milodowski, A.E., Christy, A.G., and Dodd, J. (2001) Petrographic observations of iron, copper, and zinc sulfides in freshwater canal sediment. Journal of Sedimentary Research, 71, 61–69.

Lloyd, G.E. (1987) Atomic number and crystallographic contrast images with the SEM: A review of backscattered techniques. Mineralogical Magazine, 51, 3–19.

Love, L.G. and Amstutz, G.C. (1966) Review of microscopic pyrite from the Devonian Chattanooga Shale and Rammelserg Banderz. Fortschritte der Mineralogie, 43, 277–309.

——— (1969) Framboidal pyrite in two andesites. Neues Jahrbuch fur Mineralogie. Monatshefte, 3, 97–108.

Lu, D.-L. and Tanaka, K. (1997) Different habits of Pt particles grown in salt solution at different electrode potentials. Surface Science, 373, L339–L344.

McKay, J.L. and Longstaffe, F.J. (2003) Sulphur isotope geochemistry of pyrite from the Upper Cretaceous Marshybank Formation, Western Interior Basin. Sedimentary Geology, 157, 175–195.

Muramoto, J.A., Honjo, S., Fry, B., Hay, B.J., Howarth, R.W., and Cisne, J.L. (1991) Sulfur, iron and organic carbon fluxes in the Black Sea: sulfur isotopic evidence for origin of sulfur fluxes. Deep-Sea Research, 38, S1151–S1187.

Ohfuji, H. (2004) Framboids. Ph.D. Thesis, Cardiff University, U.K.

Ohfuji, H. and Akai, J. (2002) Icosahedral domain structure of framboidal pyrite. American Mineralogist, 87, 176–180.

Ohfuji, H. and Rickard, D. (2005) Experimental syntheses of framboids—A review. Earth-Science Reviews, 71, 147–170.

Ostwald, J. and England, B.M. (1977) Note on framboidal pyrite from Allandale, New South Wales, Australia. Mineralium Deposita, 12, 111–116.

Perry, K.A. and Pedersen, T.F. (1993) Sulphur speciation and pyrite formation in meromictic ex-fjords. Geochimica et Cosmochimica Acta, 57, 4405–4418.

Prior, D.J., Trimby, P.W., Weber, U.D., and Dingley, D.J. (1996) Orientation contrast imaging of microstructures in rocks using forescatter detectors in the scanning electron microscope. Mineralogical Magazine, 60, 859–869.

Prior, D.J., Boyle, A.P., Brenker, F., Cheadle, M.C., Day, A., Lopez, G., Peruzzo, L., Potts, G.J., Reddy, S., Spiess, R., Timms, N.E., Trimby, P., Wheeler, J., and Zetterstrom, L. (1999) The application of electron backscatter diffraction and orientation contrast imaging in the SEM to textural problems in rocks. American Mineralogist, 84, 1741–1759.

Prior, D.J., Wheeler, J., Peruzzo, L., Spiess, R., and Storey, C. (2002) Some garnet microstructure: an illustration of the potential of orientation maps and misorientation analysis in microstructural studies. Journal of Structural Geology, 24, 999–1011.

Raiswell, R. and Berner, R.A. (1985) Pyrite formation in euxinic and semi-euxinic environments. American Journal of Science, 285, 710–724.

Rickard, D.T. (1970) The origin of framboids. Lithos, 3, 269–293.

Ross, D.A. and Degens, E.T. (1974) Recent sediments of the Black Sea. In E.T. Degens and D.A. Ross, Eds., Black Sea-Geology, Chemistry, and Biology. American Association of Pettoleum Geologist Memoir, 20, 183–199.

Sauter, H., Gleiter, H., and Baro, G. (1977) The effect of solute atoms on the energy and structure of grain boundaries. Acta Metallurgica, 25, 427–473.

Sawlowicz, Z. (2000) Framboids: From their origin to application. Prace Mineralogiczne, no. 88, Polska Akademia Nauk, Krakow.

Saylor, D.M. and Rohrer, G.S. (1999) Measuring the influence of grain boundary misorientation groove geometry in ceramic polycrystals. Journal of the American Ceramic Society, 82, 1536.

Spiegelmann, F. and Poteau, R. (1992) Monte-Carlo geometry optimization of

sodium clusters with a distance-dependent monoelectronic hamiltonian. In P. Jena, S.N. Khanna, and B.K. Rao, Eds., Physics and Chemistry of Finite Systems: from Cluster to Crystals, 1, 465–470. Kluwer, Dordrecht.

Spiess, R., Peruzzo, L., Prior, D.J., and Wheeler, J. (2001) Development of garnet porphyroblasts by multiple nucleation, coalescence and boundary misorientation-driven rotations. Journal of Metamorphic Geology, 19, 269–290.

Stakes, D.S., Orange, D., Paduan, J.B., Salamy, K.A., and Maher, N. (1999) Cold-seeps and authigenic carbonate formation in Monterey Bay, California. Marine Geology, 159, 93–109.

Strunz, H. (1957) Mineralogische Tabellen. Geest and Portig, Leipzig.

Suits, N.S. and Wilkin, R.T. (1998) Pyrite formation in the water column and sediments of a meromictic lake. Geology, 26, 1099–1102.

Sutton, A.P. and Baluffi, R.W. (1987) On geometric criteria for low interfacial energy. Acta Metallurgica, 35, 2177–2201.

Sweeney, R.E. and Kaplan, I.R. (1973) Pyrite framboid formation: Laboratory synthesis and marine sediments. Economic Geology, 68, 618–634.

Trimby, P.W. and Prior, D.J. (1999) Microstructural imaging techniques: a comparison of optical and scanning electron microscopy in the study of deformed rocks. Tectonophysics, 303, 71–81.

Wheeler, J., Prior, D.J., Jiang, Z., Spiess, R., and Trimby, P.W. (2001) The petrological significance of misorientations between grains. Contributions to Mineralogy and Petrology, 141, 109–124.

Wilkin, R.T. and Barnes, H.L. (1996) Pyrite formation by reactions of iron mono-sulfides with dissolved inorganic and organic sulfur species. Geochimica et Cosmochimica Acta, 60, 4167–4179.

——— (1997) Formation processes of framboidal pyrite. Geochimica et Cosmochimica Acta, 61, 323–339.

Yacaman, M.J., Ascencio, J.A., and Gardea-Torresdey, J. (2001) Structure shape and stability of nanometric sized particles. Journal of Vacuum Science and Technology, 19, 1091–1003.

MANUSCRIPT RECEIVED OCTOBER 5, 2004
MANUSCRIPT ACCEPTED MARCH 20, 2005
MANUSCRIPT HANDLED BY LEE GROAT